Disorder and nonradiative decay of Cr^{3+}-doped glasses

B. Henderson, M. Yamaga,* Y. Gao, and K. P. O'Donnell
Department of Physics and Applied Physics, University of Strathclyde, Glasgow G4 0NG, United Kingdom
(Received 30 September 1991; revised manuscript received 4 February 1992)

This paper describes experimental studies of the distributions of ligand field sites occupied by Cr^{3+} dopant ions in inorganic glasses with different chemical compositions. The effects of site-to-site disorder are observed via the steady-state spectral band-shape and decay patterns of $^4T_2 \rightarrow {}^4A_2$ and $^2E \rightarrow {}^4A_2$ transitions of Cr^{3+} ions and their temperature dependences. The temperature dependence of the emission band shape, calculated on the assumption that the disorder distribution function is a Gaussian, agrees well with the experimental results. In addition, the peak wavelengths of the $^4T_2 \rightarrow {}^4A_2$ broadbands of Cr^{3+} in different glasses are shifted to shorter wavelengths with increasing temperature, and the total intensities of the bands are reduced. These results are explained in terms of nonradiative decay of Cr^{3+} ions occupying weaker crystal-field sites.

I. INTRODUCTION

Cr^{3+} ions prefer to occupy approximately octahedral symmetry sites in inorganic crystals, in which the energy-level structure is determined by the relative strengths of the octahedral crystal field, Dq, and the interelectron interaction parameters, B and C. Solutions to the multielectron crystal-field Hamiltonian are represented on Tanabe-Sugano diagrams, in which the normalized multiplet energies, $E(\Gamma)/B$, are plotted as a function of Dq/B, for constant value of C/B, Γ denoting the irreducible representation of the electronic state.[1,2] The ground state is always the orbital singlet, $^4A_2$, irrespective of the strength of the octahedral field. In weak crystal-field sites, where $Dq/B \ll 2.3$, the lowest excited state is an orbital triplet $^4T_2$, from which broadband photoluminescence is observed due to vibronically enhanced $^4T_2 \rightarrow {}^4A_2$ transitions. For strong crystal fields ($Dq/B \gg 2.3$), the lowest excited state is changed to ^2E and the spectrum consists of narrow zero-phonon lines (R lines) with vibrationally induced sidebands due to $^2E \rightarrow {}^4A_2$ transitions. For intermediate crystal fields ($Dq/B \simeq 2.3$), mixing between $^4T_2$ and ^2E occurs: the observed photoluminescence spectrum, even at low temperature is a superposition of the broad $^4T_2 \rightarrow {}^4A_2$ band on the $^2E \rightarrow {}^4A_2$ R line and its vibronic sideband.[3–7]

Structural differences between crystals and glasses are associated with site-to-site disorder of the crystal-field sites present in the glasses. Silicate glasses are a random network of $(SiO_4)^{2-}$ tetrahedra, to which modifiers such as Li_2O, Na_2O, or K_2O are added to break up the networks. Stabilizers such as Al_2O_3 or B_2O_3 are added to prevent crystallization. Breakage of the Si—O covalent bonds by the modifier ions produces approximately octahedral arrangements of ligand ions (e.g., O^{2-}). Cr^{3+} ions prefer to occupy these octahedral sites rather than tetrahedrally coordinated sites. The octahedral crystal field at the sites occupied by Cr^{3+} ions depend strongly on randomization, which is determined by the type of modifier and stabilizer cations and their relative sizes and concentrations. In consequence, the strength of the octahedral crystal field, $10Dq$, in glassy solids varies from point to point. The spectral signatures of this disorder for a range of Cr^{3+}-doped glasses are inhomogeneously broadened absorption and emission line shapes and nonexponential decay of the Cr^{3+} luminescence.[8–12]

This paper is an extension of the earlier work by the authors, which reported spectroscopic properties of Cr^{3+}-doped fluoride, phosphate, silicate, tellurite, and borate glasses with compositions chosen to vary the mean-crystal field systematically in the range $1.8 < Dq/B < 2.3$.[8–10] The low temperature emission spectrum of Cr^{3+} in fluoride glasses, where $Dq/B \simeq 1.84$, consists of the broad $^4T_2 \rightarrow {}^4A_2$ band alone. In contrast,

TABLE I. Compositions of Cr^{3+}-doped glasses.

Glass	Composition (mol %)				
Fluoride (G8197)	8.4MgF_2	13.7SrF_2	5.1BaF_2	12.5CaF_2	17.0AlF_3
	37.6LiF	3.0$Al(PO_3)_3$	2.65Al_2O_3	0.05CrF_3	
Silicate (G8035)	68.6SiO_2	15.8Li_2O	10.7CaO	4.87Al_2O_3	0.03Cr_2O_3
Silicate (ED-2)	60.0SiO_2	27.3Li_2O	10.0CaO	2.5Al_2O_3	0.15CeO
	0.05Cr_2O_3				
Li-borate (G8382)	54.4B_2O_3	41.9Li_2O	3.6MgO	0.1Cr_2O_3	

the luminescence from Li-borate glasses, where $Dq/B \simeq 2.25$, is a superposition of the broadband ${}^4T_2 \rightarrow {}^4A_2$ spectrum and the R lines with their phonon-assisted sidebands. The total intensities of the emission spectra of Cr^{3+} in the above glasses showed strong temperature dependences due to the nonradiative decay to the ground state.

The four glasses used in the present study have compositions listed in Table I: they provide individually for a distribution of Dq values over a narrow range and, collectively, for a variation in the mean value of Dq between particular glasses. These glasses were selected from the more comprehensive set of glasses discussed recently by the authors.[8,9] The purpose of the present work is to construct a model of the energy-level structure in terms of a distribution of crystal-field sites and to use this model to calculate the optical band shape and decay characteristics of Cr^{3+} ions in these disordered environments. Having constructed the theoretical model, experimental and theoretical band shapes are compared to determine the widths of the crystal-field distributions in the different glasses. Finally, the distributions of crystal-field sites are related to structural properties of the glasses through their different chemical compositions.

II. THEORETICAL BACKGROUND

A. Absorption and emission line shapes for Cr^{3+} ions in disordered structures

The excited states of Cr^{3+} in octahedral sites interact with the vibrations of neighboring ligand ions because their wave functions extend toward these ligands. In the Born-Oppenheimer approximation, the excited states are represented by vibronic wave functions which have energy levels that depend strongly on the strength of the octahedral crystal field. When the ${}^2E$ and ${}^4T_2$ vibronic states of Cr^{3+} are close to degeneracy, the adiabatic approximation breaks down and these wave functions are mixed through the combined effects of spin-orbit coupling and the nuclear kinetic energy operators.[4-6] The wave-function admixture shows up in the emission spectra of Cr^{3+}-doped garnets such as Cr^{3+}:$Gd_2Sc_2Ga_3O_{12}$, which consist of sharp ${}^2E \rightarrow {}^4A_2$ and broadband ${}^4T_2 \rightarrow {}^4A_2$ transitions even at low temperatures below 30 K.[3-5] The mixed vibronic wave functions, required to account for such spectra, are linear combinations of the pure ${}^2E$ and ${}^4T_2$ vibronic wave functions, $\Psi_E(r,R), \Psi_T(r,R)$. The mixing coefficients are functions of the tunneling splitting, δ, and the energy separation, Δ, between ${}^2E$ and ${}^4T_2$ vibronic states.[4-6] The energy separation, Δ, is given by

$$\Delta = E({}^4T_2) - E({}^2E) = (10Dq - S\hbar\omega) - E({}^2E) , \quad (1)$$

where $E({}^2E)$ and $E({}^4T_2)$ are the energy levels of the pure ${}^2E$ and ${}^4T_2$ vibronic states at Cr^{3+} sites, $10Dq$ is the crystal-field splitting, S is the Huang-Rhys parameter, and $\hbar\omega$ is average phonon energy. This tunneling model was developed by the authors to account for the optical properties of Cr^{3+}-doped garnets. The theoretical problem is somewhat more complex in glasses on account of the distribution of crystal-field sites occupied by the Cr^{3+} ions.

In a previous paper,[10] the line shape of the ${}^4T_2 \rightarrow {}^4A_2$ broadband and the lifetime of the emission were calculated on the assumption that the distribution of sites occupied by Cr^{3+} ions in the glass as a function of crystal-field splitting $10Dq$ is a Gaussian: i.e., the probability that the Cr^{3+} ions occupy sites with $10Dq$ is assumed to be

$$P(10Dq) = \frac{1}{\sqrt{2\pi}\gamma} \exp\left[-\frac{[10Dq - (10Dq)_0]^2}{2\gamma^2} \right] , \quad (2)$$

where $(10Dq)_0$ is the energy of the Cr^{3+} sites with maximum probability and γ is the width of the distribution. In consequence, disorder produces a distribution of the energy levels $E({}^2E), E({}^4T_2)$, separations Δ, tunneling splittings δ, and of mixing parameters of the ${}^2E$ and ${}^4T_2$ excited states of the Cr^{3+} dopants, because of the distribution of the crystal-field splitting $10Dq$. Although disorder also affects the relaxation energy, $S\hbar\omega$, this effect is assumed to be negligibly small because $S\hbar\omega \simeq 2000\ cm^{-1}$ is so much smaller than the mean crystal-field energy, $(10Dq)_0 \simeq 16\,000\ cm^{-1}$.

The large difference in electron-phonon coupling between ground ${}^4A_2$ and excited ${}^4T_2$ states of Cr^{3+} ions leads to broadband optical transitions between these states. The band shape is determined by the overlap integral between the vibrational wave functions of the excited and ground states. Assuming strong electron-phonon coupling and taking account of the width of each phonon-assisted line, the approximate line-shape functions are[2]

$$I_{\pm}(E) = \frac{I_{\pm}^0}{\sqrt{2\pi}\Gamma} \exp\left[-\frac{(E - \varepsilon_{\pm})^2}{2\Gamma^2} \right] , \quad (3)$$

where $\varepsilon_+ = 10Dq$ and $\varepsilon_- = 10Dq - 2S\hbar\omega$ are energies corresponding to Frank-Condon transitions in absorption $(+)$ and emission $(-)$, and $2S\hbar\omega$ is the Stokes shift energy. The full width at half-maximum (FWHM) of this Gaussian is given by $(2\sqrt{2\ln 2})\Gamma$. The change in this line-shape function, Eq. (3), derives from including the disorder inherent in the function, Eq. (2), assumed to be a Gaussian for the distribution of Cr^{3+} ions in glasses.[10] The absorption line-shape function, $I_{ab}(E)$, including the effect of disorder, is a convolution of $I_+(E)$, Eq. (3), with the disorder distribution function, $P(10Dq)$, Eq. (2). The modified absorption band shape is a Gaussian with peak at energy, $(10Dq)_0$ and width, $\Gamma_{ab} = \sqrt{\Gamma^2 + \gamma^2}$.

Assuming that after absorption of light with energy E_{ex}, the excited electron immediately relaxes to the lowest vibronic level of the excited state at the same site without energy transfer to other sites, the distribution of the Cr^{3+} ions in the excited state is modified as

$$P'(E') = \frac{1}{\sqrt{2\pi}\gamma'} \exp\left[-\frac{(E' - \varepsilon_-)^2}{2\gamma'^2} \right] , \quad (4)$$

where

$$\varepsilon_- = \frac{\Gamma^2 (10Dq)_0 + \gamma^2 E_{ex}}{\Gamma^2 + \gamma^2} - 2S\hbar\omega , \quad (5)$$

where E_{ex} is the excitation energy, $2S\hbar\omega$ is the Stokes shift energy and $1/\gamma'^2=1/\gamma^2+1/\Gamma^2$. The emission line-shape function, $I_{em}(E)$ is also a convolution of $I_-(E)$, Eq. (3) with the modified distribution function, $P'(E')$, Eq. (4):

$$I_{em}(E)=I^0_{em}\int_0^\infty \frac{1}{\sqrt{2\pi}\Gamma}\exp\left[-\frac{(E-E')^2}{2\Gamma^2}\right]P'(E')dE' . \tag{6}$$

The modified emission band shape is a Gaussian with peak at energy, ε_-, Eq. (5), and width, Γ_{em}, being given in the form of $\Gamma_{em}=\sqrt{\Gamma^2+\gamma'^2}$.

B. Radiative and nonradiative decays of Cr^{3+} ions in disordered structures

The disorder distribution results in a distribution of excited-state lifetime and hence of the luminescence decay time. As the authors have shown,[5,6] the temperature dependence of the luminescence lifetime from the admixed excited states may be written in the form

$$\frac{1}{\tau}=\frac{\left[\frac{\alpha^2}{\tau_E}+\frac{\beta^2}{\tau_T}\right]+\left[\frac{\beta^2}{\tau_E}+\frac{\alpha^2}{\tau_T}\right]\exp\left[-\frac{\Delta E}{kT}\right]}{1+\exp\left[-\frac{\Delta E}{kT}\right]}+W_{nr}(T) , \tag{7}$$

where τ_E and τ_T are lifetimes of the pure vibronic ^2E and $^4T_2$ states, respectively, of Cr^{3+} ion, α and β are the mixing coefficients of $\Psi_E(r,R)$ and $\Psi_T(r,R)$ respectively, in $\Psi_1(r,R)$ and ΔE is energy separation between ^2E and $^4T_2$ states including the tunneling barrier.[10] Generally, the nonradiative decay rate, $W_{nr}(T)$, is represented by

$$W_{nr}(T)=R^2\exp[-S(1+2m)]\left[\frac{1+m}{m}\right]^{p/2}\times I_p(2S\sqrt{m(m+1)}) \tag{8}$$

with $m=[\exp(\hbar\omega/kT)-1]^{-1}$ and the phonon number $p=(10Dq-S\hbar\omega)/\hbar\omega$.[10,13,14] Disorder is assumed to influence only the values of $10Dq$, the values of S and R^2 being assumed constant. The value of p is also affected by disorder through the Dq term.

III. EXPERIMENTAL PROCEDURES

The general optical absorption and photoluminescence features of the different glasses in Table I have been discussed in detail by the authors.[8-10] Excitation wavelengths were obtained from a Spectra-Physics 2020-5 Ar^+ ion laser and a 380D rhodamine 6G ring dye laser. The laser excitation beam was mechanically chopped at frequencies ranging from 100 Hz to 3 kHz. The luminescence from the glass samples was focused onto the entry slit of a 0.5-m Jobin-Yvon scanning monochromator and detected at the exit slit using a photodetector and a Keithley 411 current amplifier. After amplification the signal was processed using a PAR 5209 lock-in amplifier and/or Stanford Research Systems SR250 boxcar averager, thereby permitting the measurement of CW luminescence spectra, luminescence excitation spectra, luminescence decay following pulsed excitation, and

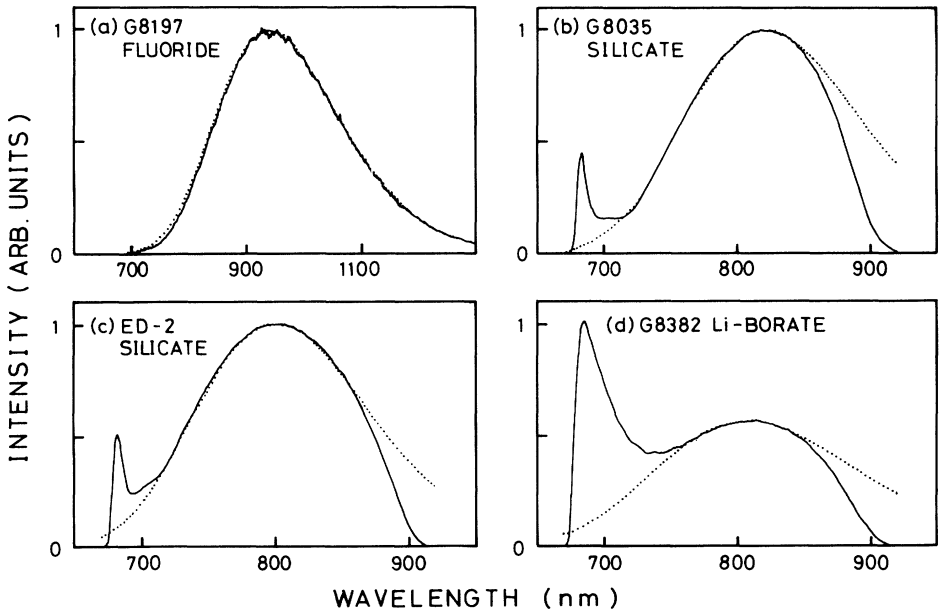

FIG. 1. Emission spectra of different Cr^{3+} doped glasses: (a) G8197 fluoride, (b) G8035 silicate, (c) ED-2 silicate, and (d) G8382 Li-borate measured at 16 K. The excitation wavelengths are 579.1 nm in (a), (b), and (c), and 581.8 nm in (d). The dotted curves are the calculated Gaussians with the fitting parameters given in Table II.

time-resolved luminescence spectra. The narrow laser linewidth of the tunable dye laser enabled fluorescence line narrowing (FLN) measurements to be made on the R lines, either in the time-resolved mode with typical delay times of 1–2 ms or by using a 90° phase shift between excitation and luminescence beams.[7–9] When a very narrow laser line is tuned to a wavelength within the inhomogeneous line profile only a small subset of sites, defined by the line profile of the laser, are excited and then reradiate at the laser wavelength. Such fluorescence line narrowing is a useful technique for measuring the homogeneous width of a transition. Apart from the narrow laser line the FLN spectrometer has all the same ingredients as an ordinary fluorescence spectrometer.[2]

The luminescence spectra of the different glasses, examples of which are given in Fig. 1, cover wide spectral ranges within the wavelength range ca. 650 nm to 1300 nm, depending upon glass composition. In consequence, two different photodetectors were employed, a Hamamatsu Photonics $R666$ GaAs photomultiplier tube for measurement at wavelengths below 900 nm, and a cooled Ge detector (North Coast Optics) when the emission intensity was significant beyond 900 nm. The photomultiplier tube has a flat response in the range of 350–840 nm, and the sensitivity is decreased by a factor of 2 at 870 nm. In consequence, when the peak wavelength is below about 820 nm (ED-2 and G8035 silicate glasses), the spectra detected by the photomultiplier reflect the real line shape except at wavelengths beyond 860 nm. However, the sensitivity of the Ge detector gradually increases from 650 to 1000 nm and is maximal at 1.5 μm, so that the broadband peaks above 830–840 nm measured with the Ge detector are shifted to longer wavelengths relative to measurements on the same glass with the photomultiplier tube. Glasses having spectra with the peak wavelengths above 850 nm (e.g., G8197 fluoride glasses) were measured using the Ge detector. The different glass samples were mounted on a cold finger in a cryorefrigerator, providing optical access to samples at working temperatures in the range 16–300 K.

IV. RESULTS

A. Emission spectra of Cr^{3+} in different glasses

Figure 1 shows representative luminescence spectra of Cr^{3+} ions in a fluoride glass (G8197), two silicate glasses (G8035 and ED-2), and a Li-borate glass (G8382). These spectra were all excited at wavelengths between 579.1 and 581.8 nm, in the long-wavelength tail of the $^4A_2 \rightarrow {}^4T_2$ absorption band. There are large variations in the ratio of intensities of the R line and broadband luminescence signals in many Cr^{3+}-doped glasses.[8,9] Generally, the G8197 fluoride glass provides low-field sites for Cr^{3+} ions; the luminescence spectrum is an isolated $^4T_2 \rightarrow {}^4A_2$ band shifted to longer wavelengths (ca. 710–1300 nm) relative to glasses containing high field sites. The other three glasses show different mixtures of R lines and broadband spectra, representing the fact that these glasses contain Cr^{3+} ions occupying both low field and high field sites. That the ratios of intensities, R lines to broadband, vary from one glass to another, shows that the mean values of Dq/B vary and that the ranges of Dq/B values are different as shown in Table II.[8,9] Dotted curves in Fig. 1 are Gaussian band shapes calculated using Eq. (6) with parameters, ε_- and Γ_{em} given in Table II. The differences between the calculated and observed spectral shapes in Figs. 1(b), 1(c), and 1(d) in the range of 670–760 nm are due to superposition of the R lines on the broadbands and above 860 nm to rapid decrease in the photomultiplier tube sensitivity.

In the absence of wave-function admixtures the decays of the $^2E \rightarrow {}^4A_2$ and $^4T_2 \rightarrow {}^4A_2$ occur on rather different time scales: the decay process may then be used to discriminate between these transitions. Figure 2 shows time-resolved emission spectra of G8382 Li-borate glass at 16 K. With zero time delay the spectrum consists of the intense R lines with their phonon sidebands and the broadband. As the delay time is increased, the intensity of the broadband, associated with Cr^{3+} in weak and intermediate field sites, decreases and is essentially zero when the delay time exceeds 1 ms. The line shown for a delay of 2 ms corresponds to Cr^{3+} in strong sites, which have the longest lifetimes. This behavior reflects the disorder distribution of the occupied Cr^{3+} site: in this glass the R line width exceeds 150 cm^{-1}, whereas in ruby it is less than 1 cm^{-1}.

This inhomogeneous broadening of the R line is confirmed by fluorescence line narrowing (FLN) measurements. Figure 3 shows typical FLN spectra of G8382 Li-borate glass. The luminescence spectrum excited in the broad $^4T_2$ absorption band at 651.3 nm is composed of the R lines with phonon sidebands due to the different Cr^{3+} sites. The FLN spectra excited at 688.2 nm and 685.4 nm are due to the $^2E \rightarrow {}^4A_2$ transition from a single Cr^{3+} site. As the excitation energy is increased, two Cr^{3+} sites with R_1 and R_2' levels resonant with the excitation energy are excited: thermal relaxation from the R_2' level at one site to its R_1' level then occurs followed by emission in the R_1' line at this site also. In consequence, the FLN spectra excited at 681.0, 677.6, and 676.5 nm

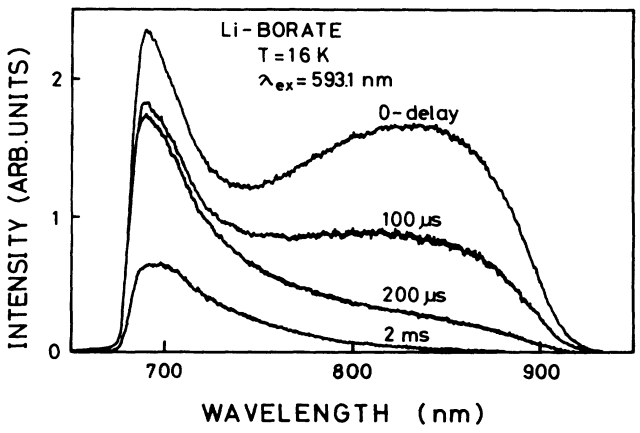

FIG. 2. Time-resolved emission spectra for G8382 Li-borate glass excited at 593.1 nm and measured at 16 K.

TABLE II. The parameters of the line-shape function.

Glass sample	Fluoride (G8197)	Silicate (8035)	Silicate (ED-2)	Li-borate (G8382)
Observed				
E_{ex} (cm^{-1})	17270	17270	17270	17190
ε_- (cm^{-1})	10620	12180	12480	12340
Γ_{em} (cm^{-1})	1200	970	1020	1150
Dq/B	1.84	2.12	2.15	2.25
Calculated				
γ^2/Γ^2	0.04	0.08	0.12	0.18
Γ (cm^{-1})	1178	935	970	1070
γ (cm^{-1})	236	260	340	445
γ' (cm^{-1})	230	255	315	420

consist of the resonant R_1 line and nonresonant R_1' line and their broadened phonon sidebands.[8,9,12] The narrowness of the homogeneously broadened FLN lines (typically 1 cm^{-1}) relative to the inhomogeneously broadened profile of the normal R line testifies to the extent of the disorder in the glass matrix.

Figure 4 shows the emission spectra of the different Cr^{3+}-doped glasses (G8197 fluoride, G8035, and ED-2 silicate, and G8382 Li-borate) excited at different laser wavelengths and measured at 16 K. The measured intensity ratio of the R line to the broadband increases both as the mean value of the crystal-field strength Dq/B in Table II and as the excitation energy increases.[8,9] The spectra in Fig. 4 show that the peak of the ${}^4T_2 \rightarrow {}^4A_2$ broadband shifts to longer wavelengths as the excitation wavelength is increased. According to Eq. (5) the peak energy, ε_-, of the broadband emission should be linearly proportional to the excitation energy, E_{ex}, with slope equal to $\gamma^2/(\Gamma^2+\gamma^2)$. The experimental results for G8382 Li-borate glass plotted in Fig. 5 are in good agreement with this prediction. The widths, γ and Γ, of the disorder distribution and the intrinsic line-shape functions may be estimated from the slope of this plot. Data for the fluoride and silicate glasses are also in good agreement with Eq. (5). The fitting-parameters, γ and Γ, for the different glasses are summarized in Table II.

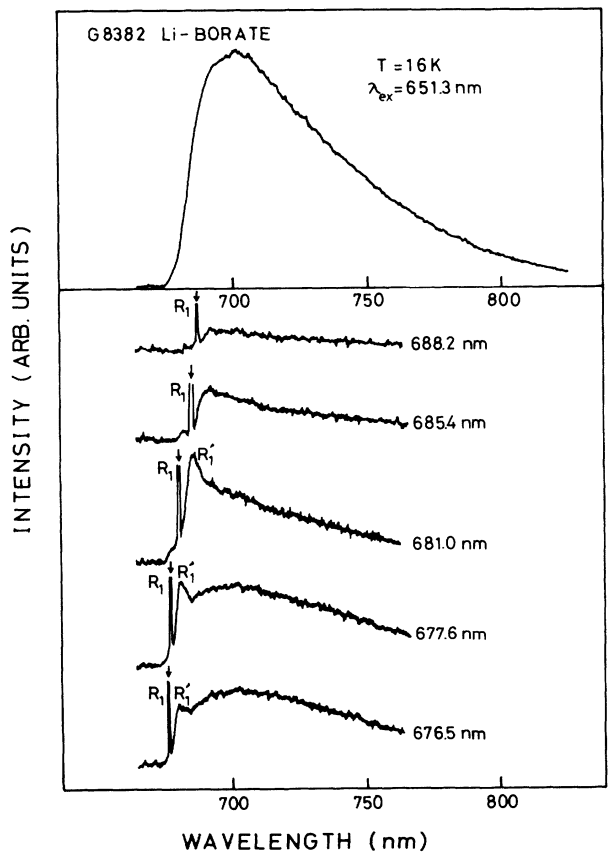

FIG. 3. Fluorescence line narrowing (FLN) spectra of G8382 Li-borate glass measured at 16 K. The arrows indicate the excitation wavelength.

B. Temperature dependence of luminescence

The luminescence lifetime, τ, varies with temperature in a complex manner in glasses because of the distribution in values of Dq. Figure 6 is a plot of theoretical values of τ versus T for the different values of $p=(10Dq-S\hbar\omega)/\hbar\omega$ in the range 34–40, calculated using Eqs. (7) and (8) assuming that the other physical parameters are set at the following values: $S=8$, $\hbar\omega=350$ cm^{-1}, $2\delta=70$ cm^{-1}, $\tau_E=6$ ms, $\tau_T=80$ μs, $E({}^2E)=14400$ cm^{-1}, and $R^2=6\times10^{14}$ s^{-1}. Nonradiative decay causes the rapid decrease of the lifetime as temperature increases, as shown in Fig. 6. Note that the values of p in the different glasses are spread out in the range 32–42 because p depends on $10Dq$, which varies from site to site in these disordered structures. Note also that the cutoff temperature, T_{cut}, defined in Fig. 6 as the temperature at which the lifetime for a particular value of p is reduced to half of the low temperature value, increases by $\sim$50 K per unit increase in p. Thus T_{cut} characterizes the nonradiative decay. These calculated curves show that Cr^{3+} ions in weak crystal-field sites (e.g., $p=34$) relax nonradiatively even at low temperature. For $p=34$ the lifetime (62 μs) at low temperature is

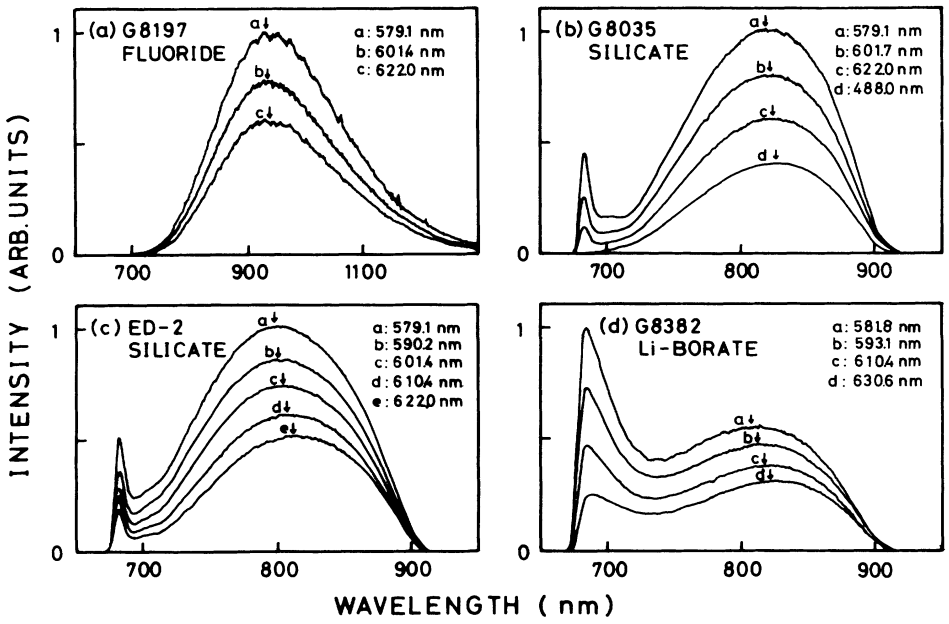

FIG. 4. Emission spectra of different Cr^{3+} doped glasses, (a) G8197 fluoride, (b) G8035 silicate, (c) ED-2 silicate, and (d) G8382 Li-borate, excited at different laser wavelengths and measured at 16 K. The arrows indicate the peaks of the emission broadbands.

smaller than that ($\tau = 80$ μs) expected of a pure $^4T_2$ state, and decreases due to increasingly probable nonradiative decay at temperatures above 80 K. As p increases in the range 34–40 the low temperature lifetime increases to 80 μs and the temperature range, over which τ is essentially constant, extends. For example, with $p = 38$, the lifetime ($\tau = 80$ μs) is invariant up to almost 300 K. At larger values of p the $^4T_2$ and ^2E levels move closer together as Dq is increased. For $p = 40$ these levels are almost degenerate. In consequence, the higher-lying ^2E level becomes increasingly populated at the expense of $^4T_2$ with increasing temperature such that the lifetime increases in the range 100–400 K; above 400 K τ decreases due to nonradiative decay.

The experimental data (open circles) superimposed on this pattern of decays are for the silicate glass G8035. A mean value of $Dq/B = 2.12$ has been reported earlier.[8] In consequence, this glass contains Cr^{3+} dopant ions occupying weak and intermediate crystal-field sites. Since the measured lifetime behavior represents a mixture of

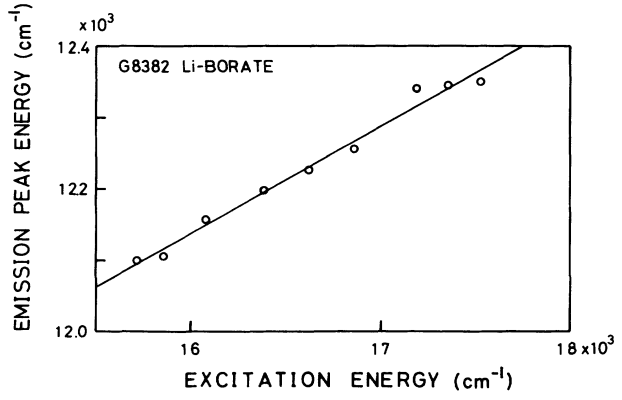

FIG. 5. The dependence of the $^4T_2 \rightarrow {}^4A_2$ emission band peak energy on the excitation energy measured for G8382 Li-borate glass at 16 K. A straight line is calculated using least squares method.

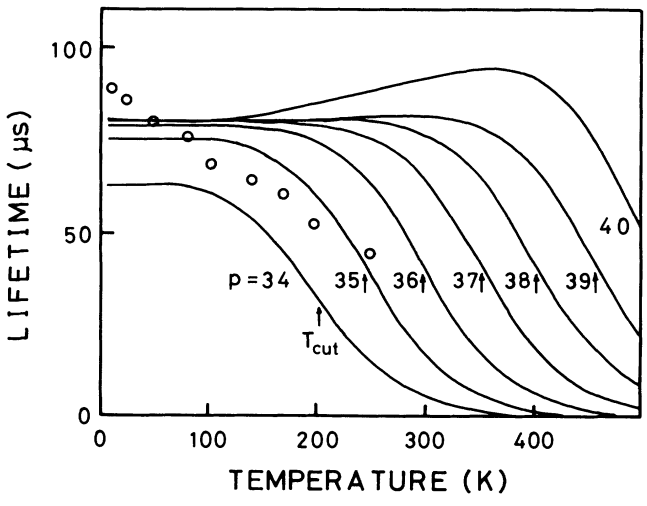

FIG. 6. Temperature dependence of the Cr^{3+} luminescence lifetime calculated including nonradiative decay terms and using Eqs. (7) and (8) assuming different values of p with physical parameters $S = 8$, $\hbar\omega = 350$ cm^{-1}, $2\delta = 70$ cm^{-1}, $\tau_E = 6$ ms, $\tau_T = 80$ μs, $E(^2E) = 14400$ cm^{-1}, and $R^2 = 6 \times 10^{14}$ s^{-1}. The Cr^{3+} luminescence lifetimes observed in G8035 silicate glass are denoted by open circles.

decays from all sites with different p values, this τ versus T plot is not expected to lie on any one of the family of curves shown in Fig. 6. Nevertheless, this comparison of theoretical and measured decay characteristics shows that it is the weak field sites (with $p \simeq 34,35$) which dominate the lifetime behavior through nonradiative decay even at low temperature. Such values of p are smaller than that estimated from the shape of the observed emission spectrum, which leads to p values spread through the range 34–38. To obtain better agreement between calculated and measured data requires an integration of Eq. (7) over the disorder distribution function and the spectrum of vibrations contributing to the nonradiative decay. Similar data are obtained for both the silicate glass ED-2 and the Li-borate glass G8382. However, the fluoride glass G8197 is predominantly a weak field glass and the lifetime decreases with increasing temperature even below 30 K.

Figure 7 shows the temperature dependence of the emission spectra of the different glasses. There are two primary effects. The total intensity of the emission band decreases gradually with increasing temperature: at 300 K the intensities are reduced to about 0.05–20 % of the intensities observed at 16 K. The wavelength at the peak of the emission band is shifted to shorter wavelength with increasing temperature. A shift in the peak of the broadband to *longer* wavelength with increasing temperature is expected as a consequence of lattice expansion. The anomalous shift to shorter wavelengths can be explained in terms of nonradiative decay, which does not occur with significant probability at low temperature (<20 K). As Fig. 6 shows the luminescence lifetime quickly decreases with increasing temperature due to nonradiative decay. The temperature dependence of the total intensity of the emission agrees with that of the lifetime on the assumption that the radiative decay rate is independent of temperature. Here, the temperature dependence of the lifetime as shown in Fig. 6 is assumed to be represented by a step function in which the lifetime is constant below the cutoff temperature, $T_{\rm cut}$ and is equal to zero above $T_{\rm cut}$. The Cr^{3+} site with phonon number, p, corresponding to a particular cutoff temperature, $T_{\rm cut}$, does not contribute to the luminescence above this temperature. A cutoff energy $\varepsilon_{\rm cut}$, associated with a peak energy of the broadband emission, is defined in terms of the phonon number, p, and Huang-Rhys parameter, S, as

$$\varepsilon_{\rm cut}=p\hbar\omega-S\hbar\omega \ . \tag{9}$$

With increasing temperature, those Cr^{3+} sites which have low emission energy, such that $\varepsilon_- \leq \varepsilon_{\rm cut}$ in Eq. (9), relax nonradiatively to the ground state above the cutoff temperature, $T_{\rm cut}$. Then, the line-shape function at temperature T including nonradiative decay effects is modified, where the range of the integration from 0 to ∞ in Eq. (6) is replaced by that from $\varepsilon_{\rm cut}$ to ∞.

The band shapes of the ${}^4T_2 \rightarrow {}^4A_2$ transition at 16 K for four glasses calculated using Eq. (6) with parameters Γ, γ, and γ' given in Table II are represented by the dotted curves in Fig. 7. The band shapes at the higher measurement temperatures are calculated using Eq. (6), with the same parameters but different integration ranges from $\varepsilon_{\rm cut}$ to ∞. The fitting parameters $\varepsilon_{\rm cut}$ and the particular measurement temperatures are summarized in Table III. We note that the peak position of the line shape is shifted to higher energy due to luminescence quenching from the weaker field sites as the temperature increases.

Figure 8 shows the total intensities, normalized to those at 16 K, measured at different temperatures and ex-

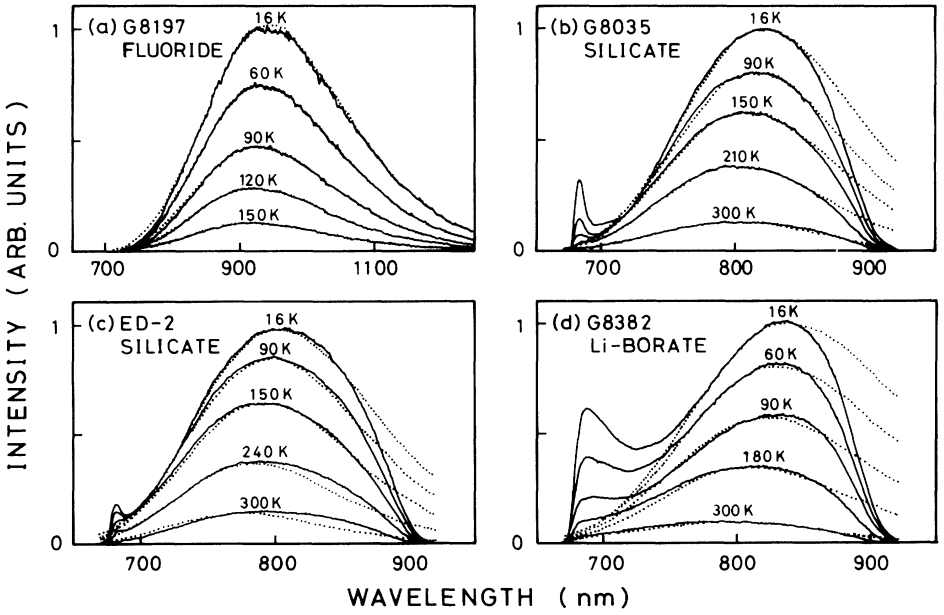

FIG. 7. The temperature dependence of the emission spectra of (a) G8197 fluoride, (b) G8035 silicate, (c) ED-2 silicate, and (d) G8382 Li-borate glasses. The dotted curves are calculated using Eq. (6) and parameters, γ', Γ in Table II and $\varepsilon_{\rm cut}$ in Table III.

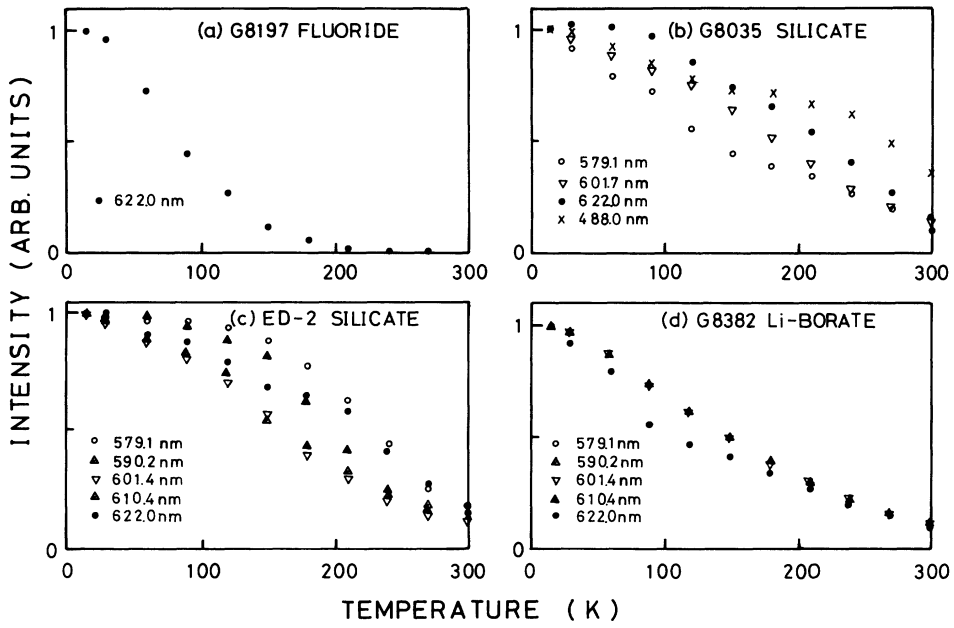

FIG. 8. The temperature dependence of the total intensity of the Cr^{3+} luminescence for different excitation wavelengths in (a) G8197 fluoride, (b) G8035 silicate, (c) ED-2 silicate, and (d) G8382 Li-borate glasses.

citation wavelengths for the different glasses. For the G8197 fluoride glass, the relative intensity starts to decrease above 40 K and is reduced to be below 0.02 at temperature above 200 K. The Cr^{3+} ions in G8197 glass occupy weak field sites and relax nonradiatively to the ground state even at low temperature as the data in Fig. 6 shows. For the silicate glasses (G8035 and ED-2), the relative intensity below 100 K is in the range of 0.8–0.9 decreasing gradually with further increase of temperature to a value of ca. 0.2 at 300 K. In contrast, the relative intensity of the strong field Li-borate glass G8382 for which $Dq/B=2.25$, decreases even at low temperature ($T=30$ K) and is reduced to 0.15 at 300 K. This can be explained in the terms of the disorder distribution function, which for G8382 Li-borate is larger than the other three glasses, the intensity reduction at low temperature being caused by the weak field Cr^{3+} sites. The average values of the relative intensities measured at 300 and 16 K excited at different laser wavelengths for the four glasses are summarized in Table IV.

A clear relationship between the excitation energy dependence, Fig. 8, and nonradiative decay was not obtained in these experiments. Nevertheless, the experimental results do indicate that the Stokes shift energy is very important for nonradiative decay, being much larger in glass samples than in the garnet crystals ($Gd_3Sc_2Al_3O_{12}$ and $Gd_3Sc_2Ga_3O_{12}$).[3,5] Nonradiative decay in the glasses from the Cr^{3+} sites with low energy $p\hbar\omega$, corresponding to weak field $10Dq$, and large Stokes shift energy $2S\hbar\omega$, occurs easily at low temperature.

TABLE III. The cutoff energy, ε_{cut}, and particular measurement temperature, T, for Cr^{3+} doped glasses.

Measurement temperature (K) \ Glass sample	Fluoride (G8197)	Silicate (8035)	Silicate (ED-2)	Li-borate (G8382)
	Cutoff energy (cm^{-1})			
60	10 240			11 390
90	10 400	11 820	11 960	11 600
120	10 520			
150	10 640	11 950	12 170	
180				11 890
210		12 110		
240			12 390	
300		12 320	12 630	12 270

TABLE IV. The ratio of the total emission intensity at 300 K to that at 16 K for different glasses.

Glass sample	Fluoride (G8197)	Silicate (8035)	Silicate (ED-2)	Li-borate (G8382)
$I(300)/I(16)$	<0.0005	0.20	0.15	0.15

V. DISCUSSION AND CONCLUSIONS

Each of the four Cr^{3+}-doped glasses discussed in this paper provides a range of octahedrally-coordinated sites for occupancy by the dopant ion. In interpreting the present spectroscopic results, as well as those in earlier publications,[8-10] the authors have considered only the distribution of the octahedral crystal field, $10Dq = 5Ze^2\langle r^4\rangle/12\pi\varepsilon_0 a^5$,[1,2] determined by the average distance, a, of the central Cr^{3+} ion and six ligand ions; the effects of symmetry lowering distortions of the octahedra are ignored. This is justified because the strength of the octahedral crystal field, $10Dq$, varies by rather more than the energy level splittings associated with nonoctahedral distortions. For example, the FLN measurements on the R lines (Fig. 3) show that the R_1-R_2 splitting measures only 50–55 cm^{-1} in the Li-borate glass whereas the disorder-induced shift in the R_1-line amounts to $\sim 150-180$ cm^{-1}. Similar FLN results have been reported for K-borate glasses[9] and for the silicate glasses G8035 and ED-2.[8,12] In accounting for the width and shape of the $^4A_2 \leftrightarrow {}^4T_2$ absorption and emission bands of Cr^{3+} ions in various glasses the authors introduced site-to-site disorder in terms of a Gaussian distribution of the octahedral crystal-field splitting, $10Dq$, Eq. (2) resulting in the line-shape function, Eq. (6), and peak position for the emission band, Eq. (5).[10]

The general spectral features of these and other glasses[8,9] were interpreted in terms of a mean value of Dq/B, disorder notwithstanding, determined from the peaks of the absorption and emission spectra. The four glasses discussed here provide a range of Dq/B values from 1.84 (fluoride) to 2.25 (Li-borate). These mean values follow trends in the anion packing densities of the glasses which increase along the series fluoride→ silicate→ borate.[9] Essentially, the greater the anion packing density, the less space is there available for the Cr^{3+} ion and the larger the value of Dq/B, although the reduced effective electron density of F^- relative to O^{2-} contributes to the weaker crystal field in fluoride glasses. For the fluoride glass G8197 the only emission component is the $^4T_2 \rightarrow {}^4A_2$ broadband, Fig. 1(a), testifying that this glass provides only low-field Cr^{3+} sites, at which the $^4T_2$ level lies lower than ^2E. The accord in Fig. 1(a) between calculated spectrum and spectrum measured at 16 K is excellent. The calculated bandwidth parameter, $\Gamma = 1178$ cm^{-1}, reflects the *homogeneous* broadening of the $^4T_2 \rightarrow {}^4A_2$ transition and is due to electron-vibrational coupling. In this glass the width of the distribution, $\gamma = 236$ cm^{-1}, is small relative to Γ.

A comparison of the line-shape and distribution functions calculated from the low temperature emission spectra for the four glasses is presented in Table II. Homogeneous broadening, Γ, of the $^4T_2 \rightarrow {}^4A_2$ transition is rather greater in the fluoride glass than in the silicate and Li-borate glasses. This may be produced by large Stokes shift for the fluoride glass. The inhomogeneous broadening is least in the fluoride glass and greatest in the borate glass. Given the narrow distribution function in the fluoride glass it is hardly surprising that the sites occupied by Cr^{3+} ions are exclusively low-field sites. The different widths of the disorder distribution in the silicate glasses G8035 (260 cm^{-1}) and ED-2 (340 cm^{-1}) follows from their different chemical compositions (Table I). The Li_2O modifier is added to break up the silicate tetrahedral network, thereby producing the approximately octahedral sites occupied by Cr^{3+} ions. Larger amounts of network modifier will result in more disorder and hence larger values of γ, in agreement with the results given in Table II for the two silicate glasses. The largest width for the distribution function is observed for the Li-borate glass. This is accounted for by the random network in borate glass consisting of trigonal and tetrahedral complexes surrounded by oxygen ligands and by very large concentration of Li_2O modifier, some 42%, used to encourage the formation of octahedral sites.[15] Given the average value of $Dq/B = 2.25$ for this glass, such a large disorder distribution requires a much larger concentration of weak-field sites than is present in the two silicate glasses.

The $^4T_2 \rightarrow {}^4A_2$ band shape at higher temperatures is also dependent upon nonradiative decay at the weaker crystal-field sites. Although odd-parity vibrations will tend to decrease the lifetime of the luminescence, such an effect will lead to an emission intensity. Since no such increase is observed in Figs. 7 and 8, it is reasonable to assume that the radiative decay rate is temperature independent. The changes in total emission intensity with increasing temperature are entirely related to nonradiative processes. In terms of the spectral band shape Eq. (6) defines a cutoff energy, ε_{cut}, such that sites which emit into broadbands with peak below ε_{cut} decay nonradiatively. Table III shows that ε_{cut} increases with increasing measurement temperature. For the fluoride glass increasing temperature from 60–150 K results in centers with peaks ranging from 977–940 nm adding to the nonradiative decay rate thereby reducing the emission intensity at longer wavelengths. The net consequence is that the peak of the emission band shifts to shorter wavelengths as the measurement temperature increases. In general, nonradiative decay is most efficient in weak-field sites. Since the fluoride glass contains only weak-field Cr^{3+} sites, nonradiative decay occurs readily even below 60 K. At 300 K the $^4T_2 \rightarrow {}^4A_2$ band is undetectable and nonradiative quenching is almost complete.

Of these four glasses the silicate glass G8035 is the most efficient emitter as illustrated in Table IV: the ratio $I(300)/I(16)$ for this glass is 0.20. This follows from the narrower distribution function, γ, of this glass relative to the silicate glass ED-2 and Li-borate glass G8382. In consequence there are comparatively fewer weak-field sites in G8035 so that nonradiative decay is less effective in decreasing the total intensity. As Table II shows the

average value of Dq for ED-2 is slightly higher than that of G8035, and this accounts for the slightly higher values of ε_{cut} for ED-2 than for G8035. However, for Li-borate glass G8382 the extreme width of the disorder distribution has the consequence that the low-field sites have a dominant effect as is indicated by the lower values of ε_{cut} relative to G8035 and ED-2 despite the larger value of Dq/B.

In conclusion, these studies have shown that the effects of the disorder structure of glasses on the $^4T_2 \rightarrow {}^4A_2$ luminescence band shape may be modeled on the assumption that the intrinsic line-shape and disorder distribution functions are Gaussians. A comparison of the measured band shape at low temperature (16 K) with the theoretical line-shape function may then be used to deduce the widths of the disorder distribution and band-shape functions. The predicted line shape at low temperature (< 16 K) agrees well with the measured shapes of $^4T_2 \rightarrow {}^4A_2$ luminescence bands in Cr^{3+}-doped fluoride, silicate, and Li-borate glasses. With increasing temperature the luminescence intensities and band shapes change as a consequence of nonradiative decay. The large Stokes shift and weak crystal field at some Cr^{3+} sites in the different glasses (Table I) enhance the nonradiative decay rate from the $^4T_2$ excited state to the $^4A_2$ ground state. The line-shape function, modified to include the effects of nonradiative decay at weak-field sites, correctly predicts the magnitude of the shift in the peak position of the $^4T_2 \rightarrow {}^4A_2$ luminescence band to shorter wavelengths with increasing temperature. The general trends in the width of the disorder distribution are in accord with the chemical compositions of the fluoride (G8197), silicate (G8035 and ED-2), and Li-borate (G8382), in particular the modifier ion content of the particular glass. The values of the cutoff energy, ε_{cut}, which defines the peak energy of the luminescence band, below which Cr^{3+} ions decay nonradiatively rather than radiatively at a particular temperature, also follow the general compositional trends. The very weak room-temperature luminescence of Cr^{3+}-doped fluoride glass is related to the exclusivity of the weak field sites available to the Cr^{3+} ions in this glass.

ACKNOWLEDGMENTS

The work was supported by SERC/MOD Grant No. GR/E 79851. The authors are indebted to Dr. S. E. Stokowski at Lawrence Livermore Laboratory who prepared the fluoride glass G8197, silicate glass G8035, and Li-borate glass G8382. The commercial silicate glass ED-2 was provided by Dr. G. F. Imbusch of University College, Galway.

*Permanent address: Department of Physics, Faculty of General Education, Gifu University, Gifu, 501-11 Japan.

[1]S. Sugano, Y. Tanabe, and H. Kamimura, *Multiplets of Transition Metal Ions in Crystals* (Academic, New York, 1970).

[2]B. Henderson and G. F. Imbusch, *Optical Spectroscopy of Inorganic Solids* (Oxford University Press, Oxford, 1989), Chap. 6.

[3]B. Struve and G. Huber, Appl. Phys. B **36**, 195 (1985).

[4]M. Yamaga, B. Henderson, and K. P. O'Donnell, J. Phys.: Condens. Matter **46**, 9175 (1989).

[5]M. Yamaga, B. Henderson, K. P. O'Donnell, C. Trager-Cowan, and A. Marshall, Appl. Phys. B **50**, 425 (1990).

[6]M. Yamaga, B. Henderson, K. P. O'Donnell, and Y. Gao, Appl. Phys. B **51**, 132 (1990).

[7]C. J. Donnelly, S. M. Healy, T. J. Glynn, G. F. Imbusch, and G. P. Morgan, J. Lumin. **42**, 119 (1988).

[8]F. Rasheed, K. P. O'Donnell, B. Henderson, and D. B. Hollis, J. Phys.: Condens. Matter **3**, 1915 (1991).

[9]F. Rasheed, K. P. O'Donnell, B. Henderson, and D. B. Hollis, J. Phys.: Condens. Matter **3**, 3825 (1991).

[10]M. Yamaga, B. Henderson, and K. P. O'Donnell, Phys. Rev. B **44**, 4853 (1991).

[11]L. J. Andrews, A. Lempicki, and B. C. McCollum, J. Chem. Phys. **74**, 5526 (1981).

[12]F. Bergin, J. F. Donegan, T. J. Glynn, and G. F. Imbusch, J. Lumin. **34**, 307 (1986).

[13]W. H. Fonger and C. W. Struck, J. Chem. Phys. **69**, 4171 (1978).

[14]R. Englman, *Non-radiative Decay of Ions and Molecules in Solids* (North-Holland, Amsterdam, 1979).

[15]R. Araujo, in *Structure and Bonding in Noncrystalline Solids*, edited by G. E. Walrafen and A. G. Revesz (Plenum, New York, 1986), pp. 13–28.